NEOPLASMA accepted, ahead of print manuscript
Cite article as https://doi.org/10.4149/neo_2026_260524N169

Running title: LAMTOR5-AS1 contributes to GBM via miR-4653-5p/TCF7 axis

LAMTOR5-AS1 predicts poor prognosis and regulates glioma progression via miR-4653-5p/TCF7 axis

Jiayi Li[1,2,3,#], Jing Li[1,2,3,#], Lin Yu[1,2,3,*]

[1]Department of Biochemistry and Molecular Biology, School of Basic Medical Sciences, Tianjin Medical University, Tianjin, China, [2]Laboratory of Molecular Immunology, Research Center of Basic Medical Science, Tianjin Medical University, Tianjin, China, [3]Tianjin Key Laboratory of Cellular and Molecular Immunology and Key Laboratory of the Educational Ministry of China, Tianjin Medical University, Tianjin, China

*Correspondence: onoblivion@tmu.edu.cn

[#]Contributed equally to this work.

Received May 24, 2026 / Accepted September 25, 2026

Gliomas, the most prevalent primary malignant brain tumors, are characterized by highly invasive growth patterns. Emerging evidence indicates that long non-coding RNAs are essential for regulating key oncogenic pathways. This study focuses on lncRNA LAMTOR5 antisense RNA AS1 (LAMTOR5-AS1, also known as SLC16A4-AS1), seeking to elucidate its regulatory functions in gliomas and assess its potential as a prognostic biomarker.
LAMTOR5-AS1 expression in normal brain tissues and glioma samples was assessed using quantitative real-time polymerase chain reaction (qRT-PCR). The Cancer Genome Atlas (TCGA) glioma dataset was mined for COX regression and Kaplan-Meier survival analyses to check LAMTOR5-AS1 correlation with clinical outcomes. The competing endogenous RNA (ceRNA) function of LAMTOR5-AS1 targeting miR-4653-5p was determined using anti-AGO2 immunoprecipitation assays and dual-luciferase reporter assays. The oncogenic properties of LAMTOR5-AS1 in glioma were systematically detected through *in vivo* and *in vitro* phenotype experiments.
The results revealed that glioma tissues had higher levels of LAMTOR5-AS1 expression, which had a positive correlation with glioma grade and indicated a poor outcome. LAMTOR5-AS1 knocking down inhibits the malignant progression of glioma cells. Mechanistically, it was demonstrated that the LAMTOR5-AS1 regulates TCF7 level via sponging miR-4653-5p, which was correlated with the malignant progression of glioma cells.
To conclude, through the miR-4653-5p/TCF7 axis, LAMTOR5-AS1 serves as ceRNA and modulates the progression of glioma.

Key words: LAMTOR5-AS1; ceRNA; glioma; prognostic biomarker

Accepted manuscript

Glioma represents the most prevalent and aggressive primary brain tumor in adults, accounting for approximately 80% of malignant central nervous system tumors [1]. Although therapeutic strategies including radiotherapy, temozolomide-based chemotherapy, and maximally safe resection have advanced significantly, the clinical outcome for glioblastoma (GBM, WHO grade 4) patients remains dismal, with a median overall survival of merely 14-16 months [2]. Nearly universal recurrence is a result of glioma cells' highly infiltrative nature and resistance to conventional therapies [3]. Molecular classification based on 1p/19q codeletion status and IDH mutation has improved prognostic stratification, but targeted therapies have shown limited clinical success [4-6]. The discovery of novel molecular regulators like lncRNAs offers opportunities for developing both diagnostic modalities and therapeutic strategies to address these unmet clinical needs in glioma management.

LncRNAs, or long non-coding RNAs, have become pivotal modulators of carcinogenesis [7], acting through diverse molecular mechanisms to influence cancer initiation [8], progression [9], and metastasis [10]. Functioning as epigenetic modulators, lncRNAs can recruit chromatin-remodeling complexes to silence tumor suppressors or activate oncogene [11-13]. They serve as ceRNAs by sponging miRNAs to derepress oncogenic mRNAs [14]. LncRNAs also modulate signaling pathways by scaffolding protein complexes [15]. The functional versatility of lncRNAs underscores their significance in cancer biology and positions them as key players in precision oncology approaches, including glioma [16]. The tissue-specific expression patterns make lncRNAs promising biomarkers for early detection and therapeutic targets in glioma [17-19].

LAMTOR5 antisense RNA AS1 (LAMTOR5-AS1, also known as SLC16A4-AS1) is genomically positioned at chromosome 1p13.3, its transcript is a new identified lncRNA. LAMTOR5-AS1 is firstly identified in prostate cancer [20]. Additional data revealed that LAMTOR5-AS1 could involve in the chemotherapy and oxidative stress process in osteosarcoma cells [21, 22]. Recent studies have showed LAMTOR5-AS1 would regulate E2F6 in non-small cell lung cancer (NSCLC) [23]. Furthermore, LAMTOR5-AS1 could also sponge miR-210-3p to regulate cervical cancer development [24].

However, the exact biological functions of LAMTOR5-AS1 in glioma pathogenesis remain inadequately characterized and warrant systematic investigation. To address this gap, our study sought to quantitatively evaluate LAMTOR5-AS1 expression patterns in glioma and determine their

Accepted manuscript

77 clinical relevance. Moreover, we systematically elucidated the functional roles and underlying
78 molecular mechanisms mediated by LAMTOR5-AS1 in glioma malignancy.
79
80 **Materials and methods**
81 **The characteristics of clinical tissue samples.** We gathered 90 glioma tissue from TMUGH
82 (Tianjin Medical University General Hospital) (see details in Supplementary Table S1). The
83 pathological diagnoses of all samples were conducted in strict accordance with the World Health
84 Organization (WHO) classification system for gliomas, with dual-pathologist verification to ensure
85 diagnostic accuracy. Ten additional non-neoplastic brain tissue samples were obtained from the
86 brain tissue of patients from TMUGH with traumatic brain injury and used as controls. The
87 TMUGH Ethics Committee examined and approved the experiment protocol, including all
88 procedures containing patient data.
89 For comparative genomic analysis, we utilized the GBM and low-grade glioma (LGG) datasets
90 from TCGA (https://cancergenome.nih.gov/). These were also used to evaluate LAMTOR5-AS1
91 expression levels and their association with clinical characteristics.
92 **Cell culture and stable cell construction.** The HEB, A172 and U251 cell lines were procured from
93 the National Biomedical Cell-Line Resource (BMCR, Beijing, China), while the U87MG and
94 HEK293T cell lines were obtained from the American Type Culture Collection (ATCC, Manassas,
95 VA, USA). All cells were cultured at 37 °C in a humidified atmosphere containing 5% CO_2 .
96 The wild-type U251 and U87MG cells were transduced with lentiviral vectors and subjected to
97 selection using 1.4 μg/ml puromycin (Solabio, Beijing, China) till stable
98 LAMTOR5-AS1-knockdown cell lines were established. The two shRNA sequences targeting
99 LAMTOR5-AS1 were as follows: LAMTOR5-AS1-sh1 (5'-ACGGATTATTCCCCTCTCGG-3')
100 and LAMTOR5-AS1-sh2 (5'-CCTCTGATGCCTTGAT-3').
101 **Transwell assay.** U251 and U87MG cells (1×10^5 /well) were seeded into Matrigel-coated
102 transwell inserts (8-μm pore size; Corning, NY, USA). Following a 12-16 h incubation period to
103 allow cellular invasion, we carefully removed the inserts and fixed them with 4% paraformaldehyde.
104 Invading cells were then stained with 0.2% crystal violet (Solabio, Beijing, China) and air-dried.
105 Quantitative analysis was performed by counting invaded cells in five randomly selected fields per
106 insert under light microscopy, with results expressed as mean number of invaded cells per field.

Accepted manuscript

107 **CCK-8 cell proliferation assay.** U251 and U87MG cells were plated and incubated for 8 h in
108 96-well plates (1×10^3 cells/well; designated as Day 0). Cell proliferation was subsequently
109 monitored daily from Day 1 to Day 5 with the Cell Counting Kit-8 (CCK-8; Dojindo, Kumamoto,
110 Japan). Utilizing a microplate spectrophotometer (Agilent Technologies, Santa Clara, CA, USA) to
111 measure the absorbance at 490 nm after incubating 1.5 h with CCK-8 reagent at 37 °C.

112 **RNA purification and qPCR.** All primers were commercially obtained from GENEWIZ (Suzhou,
113 China; sequences provided in Supplementary Table S2). TRIzol reagent (Vazyme, Nanjing, China)
114 was used to extract total RNA, followed by cDNA synthesis for both total RNA and microRNA
115 using StarScript III All-in-One RT Mix (Genstar, Beijing, China) and the miRNA 1st Strand cDNA
116 Synthesis Kit (Vazyme), respectively. Subsequently, the quantitative PCR was carried out with the
117 following cycling parameters: initial denaturation (95 °C/30 s), followed by 40 cycles were run
118 (95 °C/5 s, 60 °C/30 s). U6 and GAPDH were selected as endogenous controls to normalize miRNA
119 and mRNA expression levels, respectively. QPCR data were analyzed using the $2^{\Delta\Delta Ct}$ method.
120 GAPDH was used as the internal control for LAMTOR5-AS1 and TCF7, and U6 was used for
121 miR-4653-5p. The control group was set to 1.0, and data are presented as mean±SD from three
122 independent experiments.

123 **Western blot.** Total protein was extracted by RIPA lysis buffer (Solarbio, Beijing, China) and
124 quantified using the BCA Protein Assay Kit (Thermo Fisher Scientific, Waltham, MA, USA).
125 Subsequently, SDS-PAGE analysis was performed with 20 μg of protein loaded. Immunoblotting
126 was performed with these antibodies: anti-GAPDH (Abcam; 1:10,000) and rabbit anti-TCF7
127 (Abcam; 1:1,000). Complete antibody information is provided in Supplementary Table S3.

128 **Nuclear and cytoplasmic RNA purification assay.** Extracted RNA separately using the Nuclear
129 and Cytoplasmic RNA Purification Kit (Norgen Biotek, Thorold, ON, Canada) from 5×10^5 GBM
130 cells and synthesized the first-strand cDNA. Target transcripts were amplified using
131 LAMTOR5-AS1-specific primers under the following PCR parameters: After initial denaturation
132 (94 °C/2 min), 40 amplification cycles were run (94 °C/30 s, 60 °C/30 s, 72 °C/5 min). Internal
133 controls were the U6 snRNA and 18S rRNA.

134 **Fluorescence *in situ* hybridization (FISH).** RNA fluorescence *in situ* hybridization (RNA-FISH)
135 was performed using the Beyotime Fluorescence In Situ Hybridization Kit for RNA (#R0307)
136 according to the manufacturer's instructions. U87MG and U251 cells were seeded onto coverslips

Accepted manuscript

137 and cultured to approximately 70% confluence. Cells were fixed with 4% paraformaldehyde and
138 permeabilized with Proteinase K. Then slides were hybridized overnight in the dark with a
139 biotin-labeled probe (LAMTOR5-AS1, 5′-GTGCAGAACTCTAAGCAGGTCAT-3′) or Cy5-labeled
140 probe (miR-4653-5p, 5′-GGTGTTAAGCCTTGCTCAGAGA-3′). Following gradient washes,
141 samples were blocked with BSA and incubated with streptavidin-488 conjugate. Nuclei were
142 counterstained with DAPI, mounted in antifade mounting medium, the images were captured with a
143 fluorescence microscope. The efficiency of LAMTOR5-AS1 knockdown was determined by
144 RT-qPCR, which is the standard quantitative method for measuring lncRNA abundance. RNA-FISH,
145 when used, was applied only for subcellular localization/co-localization analysis and not for
146 quantitative assessment of knockdown efficiency.

147 **Vector construction and luciferase reporter assay.** LAMTOR5-AS1 wildtype and mutant
148 luciferase reporter vector were constructed basing on pMIR-GLO lentivirus reporter vector
149 (wild-type [WT], mutant 1 [MUT1] and mutant2 [MUT2], Promega, Madison, WI, USA). TCF7
150 wildtype 3'UTR and mutant 3'UTR sequence were also constructed in pMIR-GLO vetors
151 (WT/MUT). Two individual LAMTOR5-AS1 sh-RNA sequences were constructed in pLKO.1
152 lentivirus RNAi vector (Sigma-Aldrich, St. Louis, MO, USA) to prepare stable LAMTOR5-AS1
153 knockdown. All the vectors were constructed and sequencing verified by GENEWIZ (Suzhou,
154 China)

155 U87MG and U251 cells were transfected using Lipofectamine 3000 (Thermo Fisher Scientific,
156 Waltham, MA, USA). Cells were co-transfected with either: 1) miRNA mimics and pmirGLO-
157 LAMTOR5-AS1 constructs (wild-type [WT], mutant 1 [MUT1] and mutant2 [MUT2]) or 2)
158 miRNA mimics and pmirGLO-TCF7-3'UTR constructs (WT/MUT). Parallel transfections were
159 performed with pRL-TK and pGL3-basic plasmids in LAMTOR5-AS1 knockdown groups
160 (LAMTOR5-AS1-sh1/sh2) and control. Luciferase activity was quantified 24 h post-transfection
161 using the Luc-Pair Duo-Luciferase Assay Kit (GeneCopoeia, Rockville, MD, USA) on a GloMax
162 Navigator Microplate Luminometer (Promega, Madison, WI, USA) following manufacturers'
163 protocols.

164 **RNA immunoprecipitation (RIP) assay.** RNA-protein interactions in U251 and U87MG
165 glioblastoma cells were characterized by RIP analysis, which was carried out using the Imprint®
166 RNA Immunoprecipitation Kit (Sigma-Aldrich, St. Louis, MO, USA), following the manufacturer's

Accepted manuscript

167 protocol with modifications. Briefly, cell lysates were incubated overnight at 4 °C with 5 μg of
168 either anti-AGO2 antibody (#ab32381, Abcam, Cambridge, UK) or normal anti-IgG antibody
169 (#ab172730, Abcam), with constant rotation. The immunoprecipitated RNA was then purified for
170 use in synthesizing first-strand cDNA. Finally, quantitative and normalized analysis was performed
171 by qPCR. The data were present as relative enrichment, which refers to the fold ratio of the
172 precipitated RNA to input RNA.

173 **GBM cell line orthotopic xenograft.** For *in vitro* transduction, U87MG cells were cultured in
174 6-well plates until reaching 60-70% confluence, they were transduced with 10 μl of CON101
175 lentiviral vector (3.5×10^8 TU/ml, Ubi-MCS-firefly-Luciferase- IRES-Puromycin; GeneChem,
176 Shanghai, China) and 40 μl of 25× HiTransG Polution Enhancement Reagent (GeneChem) for 8 h
177 at 37 °C with 5% CO_2 . Transduction efficiency was verified 72 h post-infection by quantifying
178 bioluminescence signals using the IVIS Spectrum imaging system (PerkinElmer, Waltham, MA,
179 USA).

180 For *in vivo* imaging, 6-week-old male BALB/c nude mice (Vital River Laboratories) were
181 stereotactically implanted with 5×10^5 luciferase-expressing U87MG cells. After 7 days, mice
182 were performed *in vivo* bioluminescence imaging using the IVIS Spectrum system (auto-exposure,
183 8× binning, 20 cm field of view). All animal ethical procedures were approved by the Tianjin
184 Medical University Institutional Animal Care Committee.

185 **Ethics approval and consent to participate.** The research adhered to the Helsinki Declaration's
186 ethical guidelines and secured approval from the TMU Ethics Committee (Clinical sample analysis
187 Approval No.: ZYY-IRB-SOP-016(F)-00204; Animal experiments Approval No.:
188 IRB2025-DWFL-206).

189 **Statistical analysis.** To ensure methodological rigor, two independent software platforms were used
190 for all statistical analyses: 1) SPSS Statistics (version 20.0; IBM, Chicago, IL, USA) for the initial
191 analysis of clinical data, and 2) GraphPad Prism (version 9.0.0; GraphPad Software, La Jolla, CA,
192 USA) for data visualization. After Shapiro-Wilk tests confirmed normality, continuous variables
193 were expressed as mean±standard deviation (SD). Student's t-tests were employed for parametric
194 data in order to compare two groups. Multiple group comparisons were conducted taking
195 Kruskal-Wallis tests or one-way analysis of variance (ANOVA). Survival outcomes were evaluated
196 through Kaplan-Meier analysis. To ensure reproducibility, all cell-based experiments took out in

Accepted manuscript

197 triplicate biological replicates, each of which had three technical replicates. Statistical significance
198 thresholds were established as indicated below: *$p < 0.05$, **$p < 0.01$, ***$p < 0.001$, and ****$p <$
199 0.0001.
200
201 **Results**
202 **LAMTOR5-AS1 demonstrates grade-dependent overexpression in glioma and independently**
203 **predicts poor clinical outcomes.** Analysis of TCGA pan-cancer data revealed distinct expression
204 patterns of LAMTOR5-AS1 across tumor types. Compared to matched normal controls,
205 significantly elevated RNA levels of LAMTOR5-AS1 were observed in GBM, diffuse large B-cell
206 lymphoma (DLBCL), thymoma (THYM), and LGG specimens. Conversely, testicular germ cell
207 tumors (TGCT) and kidney chromophobe (KICH) exhibited marked downregulation of
208 LAMTOR5-AS1 expression. These findings, particularly the consistent overexpression in glioma
209 subtypes (GBM and LGG), suggest that dysregulated LAMTOR5-AS1 expression may acts as a
210 molecular diagnostic marker for gliomas (Figure 1A). To further explore the relationship between
211 LAMTOR5-AS1 expression and glioma WHO grading, we integrated TCGA LGG and GBM
212 datasets and performed correlation analysis. The results founded LAMTOR5-AS1 expression was
213 positively correlated with an increasing WHO grade (Figure 1B, $p < 0.001$). To confirm these
214 results, we performed qPCR analysis on an independent cohort of 90 glioma samples with varying
215 WHO grades from TMUGH, 10 non-neoplastic brain tissue samples obtained from TMUGH were
216 used as controls. Consistent with the TCGA data, LAMTOR5-AS1 expression exhibited a similar
217 grade-dependent upregulation pattern (Figure 1C, $p < 0.01$). We next examined LAMTOR5-AS1
218 expression patterns across different glioma cell lines. Compared to normal human glial cells (HEB),
219 quantitative analysis revealed significantly elevated LAMTOR5-AS1 expression levels in grade III
220 astrocytoma cell line A172 ($p < 0.05$), with the grade IV glioblastoma cell lines U87MG and U251
221 exhibiting the highest expression ($p < 0.01$). Notably, U87MG and U251 cells demonstrated
222 approximately 4-fold higher LAMTOR5-AS1 expression compared to HEB controls (Figure 1D).
223 To uncover the potential molecular mechanism of action of LAMTOR5-AS1, we initially performed
224 a fluorescence *in situ* hybridization (FISH) assay in U87MG and U251 cells, which revealed that
225 LAMTOR5-AS1 exhibits cytoplasmic predominance (Figure 1E). These findings, consistent with
226 our clinical sample data, strongly suggest that LAMTOR5-AS1 overexpression is a characteristic

Accepted manuscript

227 feature of high-grade gliomas across both patient specimens and experimental models.

228 **Elevated LAMTOR5-AS1 expression independently predicts poor prognosis in glioma**
229 **patients.** To evaluate the prognostic value of LAMTOR5-AS1 in glioma, we conducted a
230 comprehensive survival analysis using integrated TCGA datasets encompassing both lower-grade
231 glioma (LGG) and glioblastoma (GBM) patients. KM survival curves with log-rank testing
232 demonstrated patients with high LAMTOR5-AS1 levels had a notably shorter survival time
233 compared to counterparts with low-expression (Figure 2A, p=0.002). Subgroup analyses revealed
234 consistent prognostic value across histological subtypes, with high LAMTOR5-AS1 expression
235 predicting poorer OS in both LGG (Figure 2B, $p < 0.001$) and GBM (Figure 2C, p=0.035) cohorts.
236 Importantly, we observed consistent inverse correlations between LAMTOR5-AS1 expression
237 levels and disease-free survival (DFS) across all analytical cohorts: combined LGG+GBM (Figure
238 2D, p=0.004), LGG alone (Figure 2E, $p < 0.001$), and GBM alone (Figure 2F, p=0.042). The KM
239 survival results were summarized in Supplementary Table S4. These findings indicate that
240 LAMTOR5-AS1 may contribute to tumor progression.

241 Multivariate Cox regression analysis of the combined TCGA GBM+LGG cohort identified
242 LAMTOR5-AS1 expression as an independent prognostic risk factor for overall survival (Figure 2G,
243 OS, HR=1.520, 95% CI 1.058-2.183), along with WHO grade (HR=1.783, 95% CI 1.486-2.138)
244 and MKI67 expression level (95% CI 1.193-1.625, HR=1.393), while IDH mutation status served
245 as a protective factor (95% CI 0.345-0.692, HR=0.489). Notably, elevated LAMTOR5-AS1
246 expression also independently predicted shorter disease-free survival (DFS) (Figure 2H, HR=1.403,
247 95% CI 1.202-1.637), further supporting its clinical significance as a robust prognostic biomarker
248 across multiple survival endpoints.

249 **Glioma cells' malignant phenotype is facilitated by LAMTOR5-AS1.** Given the significantly
250 elevated LAMTOR5-AS1 expression levels observed in the glioblastoma cell lines U87MG and
251 U251 (Figure 1D, 4-fold higher than normal glial HEB cells, $p < 0.01$), we selected these two
252 well-characterized models for subsequent functional investigations of LAMTOR5-AS1 in glioma
253 pathogenesis. We successfully established stable LAMTOR5-AS1-knockdown U87MG and U251
254 cell lines through lentiviral shRNA transduction (sh1 and sh2). LAMTOR5-AS1 knockdown in U87
255 and U251 cells was therefore validated by RT-qPCR using GAPDH as the internal control and the
256 $2^{\Delta\Delta Ct}$ method. Compared with the scramble control, sh-LAMTOR5-AS1-1 and

Accepted manuscript

257 sh-LAMTOR5-AS1-2 reduced LAMTOR5-AS1 expression by 88% and 85% in U87 cells, and by
258 81% and 90% in U251 cells, respectively (Figure 3A, n=3 independent experiments, $p < 0.001$).
259 RNA-FISH targeting LAMTOR5-AS1 also show similar results (Supplementary Figure S1). In both
260 cell lines, CCK-8 proliferation assays demonstrated that LAMTOR5-AS1 depletion significantly
261 impaired cellular growth (Figure 3B, $p < 0.01$), while Transwell invasion assays revealed 3.2-fold
262 (U87MG) and 2.6-fold (U251) decrease in invasive capacity (Figures 3C, 3D; $p < 0.01$). For *in vivo*
263 validation, we intracranially injected luciferase-expressing U87MG scramble control or
264 LAMTOR5-AS1-sh1/2 cells (5×10^5 cells in 5 μl PBS) into six-week-old BALB/c naked mice
265 (n=5/group), with bioluminescent results showing dramatically attenuated tumor growth in
266 knockdown groups (Figures 3E, 3F, peak photon flux: 2.1×10^7 in scramble controls versus $8.7 \times$
267 10^5 and 9.4×10^5 photons/sec/cm²/steradian in LAMTOR5-AS1-sh1/2, $p < 0.001$) and KM survival
268 analysis demonstrating prolonged median survival (Figure 3G, $p < 0.01$), collectively establishing
269 LAMTOR5-AS1 as a critical regulator promoting glioma malignancy through enhancing both
270 proliferative and invasive capacities.

271 **LAMTOR5-AS1 acts as a miR-4653-5p molecular sponge.** To elucidate the molecular
272 mechanisms underlying LAMTOR5-AS1's oncogenic function, we first performed subcellular
273 fractionation experiments which confirmed its predominant cytoplasmic localization, with only
274 minimal nuclear distribution (Figure 4A). Bioinformatics analysis using two independent miRNA
275 prediction algorithms (miRanda and miRDB) identified four high-confidence candidate miRNAs
276 potentially interacting with LAMTOR5-AS1 (Figure 4B). Subsequent qRT-PCR validation in
277 LAMTOR5-AS1-knockdown U87MG and U251 cells (sh1/sh2) demonstrated significant
278 upregulation of miR-4653-5p and miR-7162-3p compared to scramble controls (Figure 4C).
279 RNA-FISH assay showed that LAMTOR5-AS1 and miR-4653-5p were co-localized mainly in the
280 cytoplasm in both U87MG and U251 cells (Supplementary Figure S2). Dual-luciferase reporter
281 assays functionally validated that miR-4653-5p mimics specifically inhibited luciferase activity in
282 wild-type LAMTOR5-AS1 constructs (25±6% reduction for U87MG and 28±2% reduction for
283 U251 vs miR-control, $p < 0.01$), while mutations in the predicted binding sites
284 (LAMTOR5-AS1-MUT1 for miR-4653-5p) abolished this suppression (Figure 4D, left panel).
285 Notably, miR-7162-3p showed no significant interaction with LAMTOR5-AS1 (Figure 4D, right
286 panel). RNA immunoprecipitation (RIP) assays, performed using anti-AGO2 antibodies,

Accepted manuscript

287 demonstrated that LAMTOR5-AS1 and miR-4653-5p were significantly co-precipitated compared
288 to the IgG controls, the relative enrichment fold ratios of the precipitated RNA (LAMTOR5-AS1,
289 miR-4653-5p or miR-7162-3p) relative to input were presented in Figure 4E ($p < 0.01$), providing
290 direct evidence for their physical interaction within the RISC complex. These thorough findings
291 demonstrate that LAMTOR5-AS1 sequesters miR-4653-5p in glioblastoma cells by acting as a
292 molecular sponge.

293 **miR-4653-5p suppresses TCF7 expression through direct 3'UTR targeting.** While previous
294 studies have not investigated the downstream targets of miR-4653-5p, we systematically identified
295 its regulatory targets through an integrated bioinformatics and experimental approach. Using
296 TargetScan algorithm, we predicted 3,090 potential mRNA targets of miR-4653-5p, which were
297 then cross-referenced with 2,096 differentially expressed genes showing significant correlation with
298 upstream lncRNA LAMTOR5-AS1 in TCGA LGG/GBM datasets ($p < 0.01$, Pearson's $r > 0.2$),
299 yielding 210 high-confidence candidate targets (Figure 5A). KEGG pathway analysis revealed
300 Wnt/β-catenin signaling as the most significantly enriched pathway (FDR < 0.001, Figure 5B).
301 Subsequent qPCR validation in miR-4653-5p-overexpressing U87MG and U251 cells demonstrated
302 TCF7 as the most downregulated among the three tested genes (Figure 5C, 3.3±0.3-fold decrease in
303 U87MG and 3.7±0.4-fold decrease in U251, $p < 0.01$), confirmed at protein level by western
304 blotting (Figure 5D, $p<0.01$). Dual-luciferase reporter assays with wild-type (WT) and mutant
305 (MUT) TCF7 3'UTR constructs showed miR-4653-5p specifically suppressed WT reporter activity
306 by 62±1% in U87MG and 78±3% in U251 (Figure 5E, $p < 0.01$) without affecting MUT controls.
307 RNA immunoprecipitation (RIP) using anti-AGO2 antibodies verified physical association between
308 miR-4653-5p and TCF7 mRNA (Figure 5F, $p < 0.01$). Comprehensive analysis of integrated TCGA
309 LGG and GBM datasets showed a notable positive correlation between LAMTOR5-AS1, the
310 upstream regulatory lncRNA of miR-4653-5p, and TCF7 transcripts (Figure 5G, $p < 0.001$). The
311 results established a previously unrecognized mechanistic demonstration that TCF7 serves as a
312 direct functional target of miR-4653-5p through both 3'UTR-mediated repression and RISC
313 complex incorporation, and LAMTOR5-AS1 might regulate TCF7 level by sponging miR-4653-5p.

314 **LAMTOR5-AS1 facilitates the malignancy phenotype of glioma cells through the**
315 **LAMTOR5-AS1/miR-4653-5p/TCF7 axis.** To functionally validate the oncogenic role of the
316 LAMTOR5-AS1/miR-4653-5p/TCF7 axis in glioblastoma pathogenesis, we performed rescue

Accepted manuscript

317 experiments using miR-4653-5p-specific antisense oligonucleotides (ASOs) in
318 LAMTOR5-AS1-knockdowned U87MG and U251 cells. Quantitative RT-PCR and immunoblotting
319 analysis demonstrated that miR-4653-5p inhibition effectively restored TCF7 expression not only at
320 mRNA but also at protein levels compared to control ASO-treated cells (Figures 6A, 6B).
321 Phenotypic characterization revealed that miR-4653-5p ASO treatment significantly rescued the
322 impaired proliferative capacity (in CCK-8 assay, $p < 0.01$) and invasive potential (in Transwell
323 assay, $p < 0.01$) induced by LAMTOR5-AS1 knockdown (Figures 6C, 6D). These comprehensive
324 findings establish that LAMTOR5-AS1 promotes glioblastoma cell malignancy through a ceRNA
325 mechanism involving miR-4653-5p sequestration and subsequent TCF7 derepression, ultimately
326 driving tumor cell proliferation and invasion (Figures 6E).
327

328 **Discussion**

329 LAMTOR5-AS1 serves as a multifaceted regulatory lncRNA with context-dependent roles in
330 various cancers [25], primarily functioning through miRNA sponging mechanisms to modulate
331 critical cellular processes [24, 26]. In osteosarcoma cells, LAMTOR5-AS1 contributes to drug
332 resistance by acting as a ceRNA that protects HNF4A mRNA from miR-34a-3p-mediated repression
333 and facilitates the SIRT1/HNF4A interaction, while also regulating chemotherapy sensitivity
334 through modulation of the NRF2/KEAP1 oxidative stress pathway [22]. The lncRNA exhibits
335 tumor-promoting activities in NSCLC cells by forming a ceRNA network with miR-506-3p to
336 regulate E2F6 expression, thereby enhancing proliferation and metastasis [23], whereas in cervical
337 cancer it appears to function as a tumor suppressor through its interaction with miR-210-3p [24].
338 LAMTOR5-AS1's clinical relevance is further supported by its identification as a diagnostic
339 biomarker in prostate cancer and its potential connection with HBXIP (LAMTOR5) in colorectal
340 cancer, where it may regulate miR-let-7b-3p and miR-20a-5p [20, 27]. Additionally, in
341 osteosarcoma, LAMTOR5-AS1 participates in pyroptosis regulation through the
342 hsa-miR-23a-3p/TP63 axis, and its differential expression patterns between chemosensitive and
343 chemoresistant cell lines suggest a role in treatment response [28].
344 To date, the expression patterns, downstream effects, and molecular mechanisms of
345 LAMTOR5-AS1 in gliomas remain unexplored. Our comprehensive analysis of both TMUGH
346 clinical specimens and TCGA datasets displayed significant overexpression of LAMTOR5-AS1 in

Accepted manuscript

347 glioma tissues, with a striking positive correlation between its expression levels and tumor grade (p
348 < 0.001, ANOVA), demonstrating peak expression in glioblastoma (GBM) samples. Most
349 importantly, univariate Cox proportional hazards regression analysis identified LAMTOR5-AS1
350 expression as a powerful independent predictor of poor clinical outcomes (HR=1.520, 95% CI
351 1.058-2.183, p=0.023 for OS, HR=1.403, 95% CI 1.202-1.637, p < 0.01 for DFS), establishing its
352 potential as a novel molecular prognostic marker for glioma patient stratification.
353 The precursor gene of miR-4653-5p, MIR4653, is located in an intergenic region of chromosome
354 7q22.1, with miR-4653-5p being processed from the 5' arm of this precursor (PubChem Substance
355 ID: 251851779; https://pubchem.ncbi.nlm.nih.gov/substance/251851779), first identified in 2015.
356 To date, the expression profile of miR-4653-5p only documented in Type 1 diabetes mellitus cells
357 [29]. While the downstream targets and molecular mechanisms of miR-4653-5p remain completely
358 uncharacterized. In this study, we present the first experimental evidence demonstrating that: 1)
359 miR-4653-5p directly targets TCF7 through 3'UTR binding, as validated by dual-luciferase reporter
360 assays and AGO2-RIP experiments; and 2) LAMTOR5-AS1 as a ceRNA, targets and modulates
361 TCF7 expression by sequestering miR-4653-5p.
362 When abnormally activated, the canonical Wnt/β-catenin signaling pathway has been demonstrated
363 to foster multiple kinds of cancer's development [30-32]. As a crucial transcriptional effector of
364 Wnt signaling, TCF7 mediates the nuclear transduction of β-catenin-dependent transcriptional
365 programs [33-35]. Our experimental data demonstrate that genetic ablation of LAMTOR5-AS1
366 substantially reduces TCF7 expression in glioma cell lines at mRNA and protein levels. Subsequent
367 functional research showed that TCF7 degradation dramatically attenuates glioma cell proliferation
368 and invasion. Most notably, our findings provide the first experimental evidence establishing a
369 mechanistic link between LAMTOR5-AS1 expression and Wnt/β-catenin pathway activation in
370 glioma pathogenesis.
371 In conclusion, our findings demonstrate that LAMTOR5-AS1 expression exhibits a significant
372 positive correlation with both WHO glioma grade and unfavorable patient outcomes, establishing
373 its potential as both molecular classifier for gliomas stratification and a novel prognostic biomarker.
374 Mechanistically, we have identified a previously unrecognized cytoplasmic function of
375 LAMTOR5-AS1 in driving glioma malignancy through its role to serve as ceRNA that sequesters
376 miR-4653-5p, reducing the suppression of TCF7 expression caused by miR-4653-5p and

Accepted manuscript

subsequently activating oncogenic signaling pathways that promote glioma progression.

Acknowledgements: The research was supported by the National Natural Science Foundation of China (No. 82072772).

Supplementary data are available in the online version of the paper.

References

[1] XIAO D, YAN C, LI D, XI T, LIU X et al. National Brain Tumour Registry of China (NBTRC) statistical report of primary brain tumours diagnosed in China in years 2019-2020. Lancet Reg Health West Pac 2023; 34: 100715. https://doi.org/10.1016/j.lanwpc.2023.100715

[2] CHEN F, WENDL MC, WYCZALKOWSKI MA, BAILEY MH, LI Y et al. Moving pan-cancer studies from basic research toward the clinic. Nat Cancer 2021; 2: 879-90. https://doi.org/10.1038/s43018-021-00250-4

[3] STUPP R, TAILLIBERT S, KANNER A, READ W, STEINBERG D et al. Effect of Tumor-Treating Fields Plus Maintenance Temozolomide vs Maintenance Temozolomide Alone on Survival in Patients With Glioblastoma: A Randomized Clinical Trial. JAMA 2017; 318: 2306-2316. https://doi.org/10.1001/jama.2017.18718

[4] HINZ F, FRIEDEL D, KORSHUNOV A, IPPEN FM, BOGUMIL H et al. IDH-mutant astrocytomas with primitive neuronal component have a distinct methylation profile and a higher risk of leptomeningeal spread. Acta Neuropathol 2025; 149: 12. https://doi.org/10.1007/s00401-025-02849-8

[5] GARCIA FOX R, CHUKWUEKE UN, SANNES T, MIRAN D, CHIU D et al. Glioma resource outreach with support: A program to identify and initiate supportive care interventions for unmet needs among adult lower-grade glioma patients. Neurooncol Pract 2025; 12: 87-99. https://doi.org/10.1093/nop/npae065

[6] LUCAS CG, AL-ADLI NN, YOUNG JS, GUPTA R, MORSHED RA et al. Longitudinal multimodal profiling of IDH-wildtype glioblastoma reveals the molecular evolution and cellular phenotypes underlying prognostically different treatment responses. Neuro Oncol 2025; 27(1): 89-105. https://doi.org/10.1093/neuonc/noae214

[7] PENG X, YANG R, WANG C, PENG W, ZHAO Z et al. The YTHDF3-DT/miR-301a-3p /INHBA axis attenuates autophagy-dependent ferroptosis in lung adenocarcinoma. Cancer Lett 2025; 613: 217503. https://doi.org/10.1016/j.canlet.2025.217503

[8] DAI L, LI J, DONG Z, LIU Y, CHEN Y et al. Temporal expression and functional analysis of long non-coding RNAs in colorectal cancer initiation. J Cell Mol Med 2019; 23: 4127-4138. https://doi.org/10.1111/jcmm.14300

[9] JIANG M, ZHANG K, WEI G, QI F, YU D et al. HDAC4 super-enhancer drives CEBPB-mediated TWIST2 transcription to promote chemoresistance in LUAD. Cancer Lett 2025; 623: 217716. https://doi.org/10.1016/j.canlet.2025.217716

Accepted manuscript

[10] ZHOU JM, DAI WX, WANG RJ, XU WQ, XIANG Z et al. Organoid modeling identifies USP3-AS1 as a novel promoter in colorectal cancer liver metastasis through increasing glucose-driven histone lactylation. Acta Pharmacol Sin 2025; 46: 1404-1418. https://doi.org/10.1038/s41401-024-01465-8

[11] DAI C, QIANJIANG H, FU R, YANG H, SHI A et al. Epigenetic and epitranscriptomic role of lncRNA in carcinogenesis (Review). Int J Oncol 2025; 66: 29. https://doi.org/10.3892/ijo.2025.5735

[12] ABDELNEAM AI, MOHAMMED GF. Non-coding RNAs (miRNAs - circRNAs - lncRNAs) and genes interact with the regulation of vitiligo. Arch Dermatol Res 2025; 317: 679. https://doi.org/10.1007/s00403-025-04113-1

[13] ZHANG X, SHI L, XING M, LI C, MA F et al. Interplay between lncRNAs and the PI3K/AKT signaling pathway in the progression of digestive system neoplasms (Review). Int J Mol Med 2025; 55: 15. https://doi.org/10.3892/ijmm.2024.5456

[14] GE L, MA J, XU J, WANG B, ADIL A et al. The mechanism of lncRNA PVT1 targeting the miR-30a/Beclin-1 axis to mediate ventricular remodeling in spontaneously hypertensive rats. Cell Signal 2025; 130: 111650. https://doi.org/10.1016/j.cellsig.2025.111650

[15] WU W, LI X, ZHAO J, GUI Y, LUO Y et al. The Role of Long Non-Coding RNF144A-AS1 in Cancer Progression. Cell Biochem Biophys 2024; 82: 2007-2017. https://doi.org/10.1007/s12013-024-01411-9

[16] FENG C, LI Q, LV M, JI Q, YE H et al. A pan-cancer analysis of small nucleolar RNA host gene 14 (SNHG14) in human tumors. Gene 2025; 951: 149410. https://doi.org/10.1016/j.gene.2025.149410

[17] FANG Z, PAN Y, LU Z, WANG L, HU X et al. LncRNA SNHG1: A novel biomarker and therapeutic target in hepatocellular carcinoma. Gene 2025; 958: 149462. https://doi.org/10.1016/j.gene.2025.149462

[18] CHEN B, YUAN S, WANG H. Identification of a cuproptosis- related prognostic biomarker and therapeutic target in ovarian cancer. Oncol Lett 2025; 29: 302. https://doi.org/10.3892/ol.2025.15048

[19] PAN Y, ZHANG Y, HU X, LI S. Construction of a Novel Cuproptosis-Related ceRNA Network-SNHG3/miR-1306-5p/PDHA1 and Identification of SNHG3 as a Prognostic Biomarker in Hepatocellular Carcinoma. ACS Omega 2023; 8: 38690-38703. https://doi.org/10.1021/acsomega.3c06018

[20] LI Z, ZHENG J, XIA Q, HE X, BAO J et al. Identification of Specific Long Non-Coding Ribonucleic Acid Signatures and Regulatory Networks in Prostate Cancer in Fine-Needle Aspiration Biopsies. Front Genet 2020; 11: 62. https://doi.org/10.3389/fgene.2020.00062

[21] PU Y, TAN Y, ZANG C, ZHAO F, CAI C et al. LAMTOR5-AS1 regulates chemotherapy-induced oxidative stress by controlling the expression level and transcriptional activity of NRF2 in osteosarcoma cells. Cell Death Dis 2021; 12: 1125. https://doi.org/10.1038/s41419-021-04413-0

[22] ZHAO F, WEI C, PU Y, ZANG C. LAMTOR5-AS1 Regulates Chemotherapy-induced Oxidative Stress via the miR-34a-3p/SIRT1/HNF4A Axis in Osteosarcoma Cells. Curr Med Chem 2025; 32: 6633-6645. https://doi.org/10.2174/0109298673316534240708111058

[23] CHEN G, WANG K, LI G, WANG L, XIAO Y et al. Long Noncoding RNA LAMTOR5-AS1 Interference Affects MicroRNA-506-3p/E2F6-Mediated Behavior of

Accepted manuscript

Non-Small Cell Lung Cancer Cells. Oncol Res 2022; 28: 945-959. https://doi.org/10.3727/096504021x16328213967104

[24] YANG B, WANG Z, DENG Y, XIAO L, ZHANG K. LncRNA LAMTOR5-AS1 sponges miR-210-3p and regulates cervical cancer progression. J Obstet Gynaecol Res 2022; 48: 3171-3178. https://doi.org/10.1111/jog.15439

[25] WANG Y, XIE Q, YU H, ZHOU B, GUO X et al. Establishment and validation of the autophagy-related ceRNA network in irreversible pulpitis. BMC Genomics 2023; 24: 268. https://doi.org/10.1186/s12864-023-09363-9

[26] ZANIANI NR, OROUJALIAN A, VALIPOUR A, PEYMANI M. LAMTOR5 expression level is a biomarker for colorectal cancer and lncRNA LAMTOR5-AS1 predicting miRNA sponging effect. Mol Biol Rep 2021; 48: 6093-6101. https://doi.org/10.1007/s11033-021-06623-3

[27] ABKENAR BR, MOHAMMADI A, AMOLI HA, SOLEIMANI AA, KORANI M et al. Non-coding RNAs are correlated to TGF-beta receptor type 2 in patients with colorectal cancer. J Gene Med 2023; 25: e3472. https://doi.org/10.1002/jgm.3472

[28] HAN J, HU Y, DING S, LIU S, WANG H. The analysis of the pyroptosis-related genes and hub gene TP63 ceRNA axis in osteosarcoma. Front Immunol 2022; 13: 974916. https://doi.org/10.3389/fimmu.2022.974916

[29] YI X, CHENG X. Understanding Competitive Endogenous RNA Network Mechanism in Type 1 Diabetes Mellitus Using Computational and Bioinformatics Approaches. Diabetes Metab Syndr Obes 2021; 14: 3865-3945. https://doi.org/10.2147/dmso.S315488

[30] ZHU F, YAN HHN, TONG Y, ZHAO Y. Exploring WNT pathway dysregulation in serrated colorectal cancer for improved diagnostic and therapeutic strategies. Front Genet 2025; 16: 1586867. https://doi.org/10.3389/fgene.2025.1586867

[31] HAN J, YUAN Y, ZHANG J, HOU Y, XU H et al. Regulatory effect of Wnt signaling on mitochondria in cancer: from mechanism to therapy. Apoptosis 2025; 30: 1235-1252. https://doi.org/10.1007/s10495-025-02114-z

[32] NADIN SB, CUELLO-CARRION FD, CAYADO-GUTIERREZ N, FANELLI MA. Overview of Wnt/beta-Catenin Pathway and DNA Damage/Repair in Cancer. Biology (Basel) 2025; 14: 185. https://doi.org/10.3390/biology14020185

[33] YE B, LI L, XU H, CHEN Y, LI F. Opposing roles of TCF7/LEF1 and TCF7L2 in cyclin D2 and Bmp4 expression and cardiomyocyte cell cycle control during late heart development. Lab Invest 2019; 99: 807-818. https://doi.org/10.1038/s41374-019-0204-2

[34] LI Q, HUA Y, YANG Y, HE X, ZHU W et al. T Cell Factor 7 (TCF7)/TCF1 Feedback Controls Osteocalcin Signaling in Brown Adipocytes Independent of the Wnt/beta-Catenin Pathway. Mol Cell Biol 2018; 38: e00562. https://doi.org/10.1128/MCB.00562-17

[35] ZHAN Y, FENG J, LU J, XU L, WANG W et al. Expression of LEF1 and TCF1 (TCF7) proteins associates with clinical progression of nasopharyngeal carcinoma. J Clin Pathol 2019; 72: 425-430. https://doi.org/10.1136/jclinpath-2019-205698

Figure Legends

Figure 1. LAMTOR5-AS1 levels are correlated with glioma WHO grades A) The pan-cancer atlas depicting LAMTOR5-AS1 transcripts per million (TPM) in multiple tissues. B) Differential

Accepted Manuscript

506 expression of LAMTOR5-AS1 across glioma grades based on TCGA datasets (control=105). C)
507 The expression level of LAMTOR5-AS1 in TMUGH samples with different glioma grades
508 (control=20). (D) The LAMTOR5-AS1's relative mRNA levels in human astrocyte (HEB) cells and
509 glioma cells (U87MG, U251, A172). (E)RNA- FISH was performed to visualize the intracellular
510 localization of LAMTOR5- AS1 (green), DAPI was used to stain cell nuclei (blue). *p < 0.05; **p
511 < 0.01; ***p < 0.001
512
513 **Figure 2.** LAMTOR5-AS1 expression as a clinical prognostic biomarker in glioma. A)
514 Kaplan-Meier (KM) analysis was performed on the overall survival (OS) time of TCGA-LGG and
515 TCGA-GBM samples (n=603) with samples stratified by LAMTOR5-AS1 expression levels. B) OS
516 was assessed by KM analysis in TCGA-LGG samples (n=473) categorized according to
517 LAMTOR5-AS1 expression. C) KM analysis of OS in TCGA-GBM samples (n=130) stratified by
518 LAMTOR5-AS1 expression D-F) Using a stratification approach based on LAMTOR5-AS1
519 expression levels, we performed KM analysis to evaluate disease-free survival (DFS) in
520 LGG+GBM (D) or LGG (E) or GBM (F) samples from the TCGA dataset. G) A forest plot was
521 utilized to show how the OS was affected by the LAMTOR5-AS1 RNA expression level in the
522 LGG+GBM datasets from TCGA. H) A forest plot was utilized to show how the DFS in the TCGA
523 GBM datasets was affected by the levels of LAMTOR5-AS1 RNA expression.
524
525 **Figure 3.** LAMTOR5-AS1 knockdown suppresses GBM malignancy *in vitro* and *in vivo*. A)
526 LAMTOR5-AS1 knockdown in U251 and U87MG cells was confirmed by qRT-PCR results (n=3).
527 B) Following LAMTOR5-AS1 knockdown (n=3), GBM cells proliferation was measured by
528 performing CCK-8. C-D) The invasive capacity of LAMTOR5-AS1-knockdown GBM cells was
529 evaluated using Transwell assays (n=3). E) Representative bioluminescent pictures of xenograft
530 tumors in BALB/c naked mice in the shLAMTOR5-AS1 groups (LAMTOR5-AS1-sh1 and
531 LAMTOR5-AS1-sh2) and U87MG control group (Scramble). F) Corresponding photon flux
532 quantification in BALB/c naked mice. (n=5). G) Kaplan-Meier survival analysis of the control
533 group and LAMTOR5-AS1 sh1/sh2 group in glioblastoma mouse models. (n=5/group). *p < 0.05;
534 **p < 0.01; ***p < 0.001. Data are expressed as the mean±SD.
535

Accepted manuscript

536 **Figure 4.** LAMTOR5-AS1 plays a sponge role for miR-4653-5p. A) Subcellular distribution of
537 LAMTOR5-AS1 in GBM cells (U87MG and U251) were analyzed by qPCR. B) The miRNAs
538 which were identified as possibly binding to LAMTOR5-AS1 were those predicted by both
539 miRanda (n=45) and miRDB (n=19). C) qRT-PCR analysis demonstrated altered miRNA
540 expression levels in GBM cells following LAMTOR5-AS1 knockdown (U87MG and U251 cells).
541 D) The luciferase reporter plasmids are shown schematically, with one containing the miRNA
542 sequence for the LAMTOR5-AS1 interaction and the other without (upper panel). The targeting
543 relationship between LAMTOR5-AS1 and either miR-4653-5p or miR-7162-5p was demonstrated
544 by the dual-luciferase reporter assay (lower panel). E) U87MG and U251 cells were subjected to an
545 Anti-AGO2 RIP test, followed by a qRT-PCR assay to determine AGO2's enrichment capacity on
546 LAMTOR5-AS1, miR-4653-5p, or miR-7162-5p in comparison to IgG. **$p < 0.01$; ***$p < 0.001$
547
548 **Figure 5.** LAMTOR5-AS1 modulates the Wnt signaling pathway via sponging miR-4653-5p. A)
549 The overlap analysis between genes significantly correlated with upstream LAMTOR5-AS1 in
550 TCGA LGG+GBM datasets (n=2096) and miR-4653-5p-targeting genes predicted by TargetScan
551 (n=3090). B) Gene Ontology enrichment analysis results for overlapping genes, presented as a
552 bubble plot (n=210). C, D) Relative expression of TCF7, WNT9A and WNT9B was detected by
553 qPCR (C), while western blot was performed to quantify TCF7 protein levels following transfection
554 with the mimics of miR-4653-5p (D). E) Luciferase activities were determined in U87MG and
555 U251 cell lines following co-transfection with either WT/MUT-TCF7 3'UTR constructs, and
556 mimic-control or miR-4653-5p mimics. F) AGO2-RIP assays confirmed that miR-4653-5p and
557 TCF7 interact. G) Correlation analysis of LAMTOR5-AS1 and TCF7 expression in TCGA LGG
558 and GBM datasets. **$p < 0.01$
559
560 **Figure 6.** Malignant GBM cell phenotype is promoted by LAMTOR5-AS1 via
561 LAMTOR5-AS1/miR-4653-5p/TCF7 axis. A, B) qPCR and western blot showing altered TCF7
562 expression levels in U251 and U87MG cells post-treatment with miR-4653-5p-specific ASOs. The
563 relative expression of TCF7 was calculated using the 2ΔΔCt method. The scramble+control ASO
564 group was used as the calibrator and set to 1.0 (leftmost red bar). C) Results of cell proliferation
565 assays using miR-4653-5p-specific ASO (n=3). D) Transwell assays illustrating the invasion

Accepted manuscript

566 capability among the GBM cells (n=3). E) The schematic diagram illustrates the potential
567 mechanism by which LAMTOR5-AS1 promotes the malignancy of glioblastoma. *$p < 0.05$; **$p <$
568 0.01. Data are presented as mean±SD.

Accepted manuscript

Fig. 1 Download full resolution image

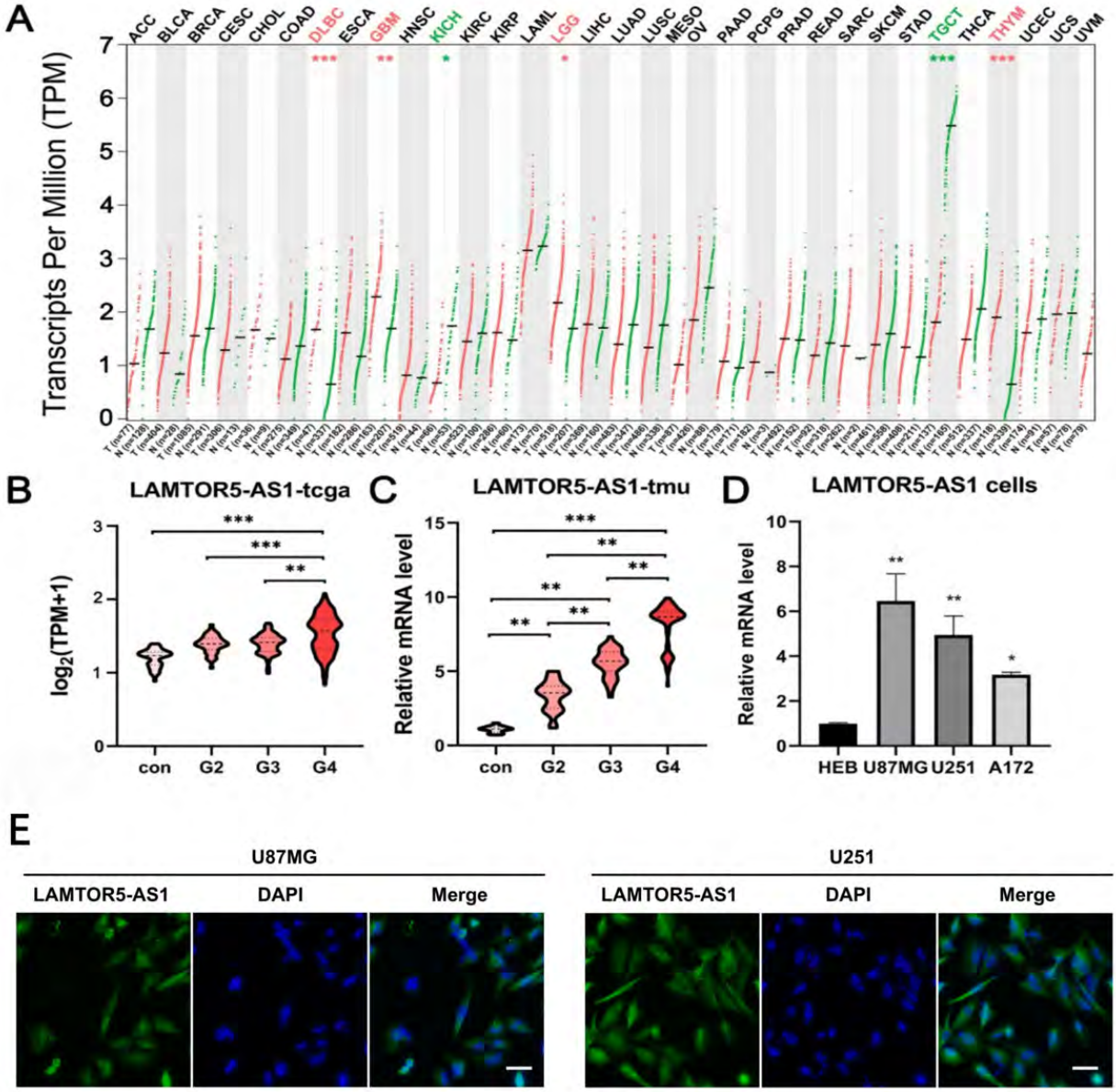

Fig. 2 Download full resolution image

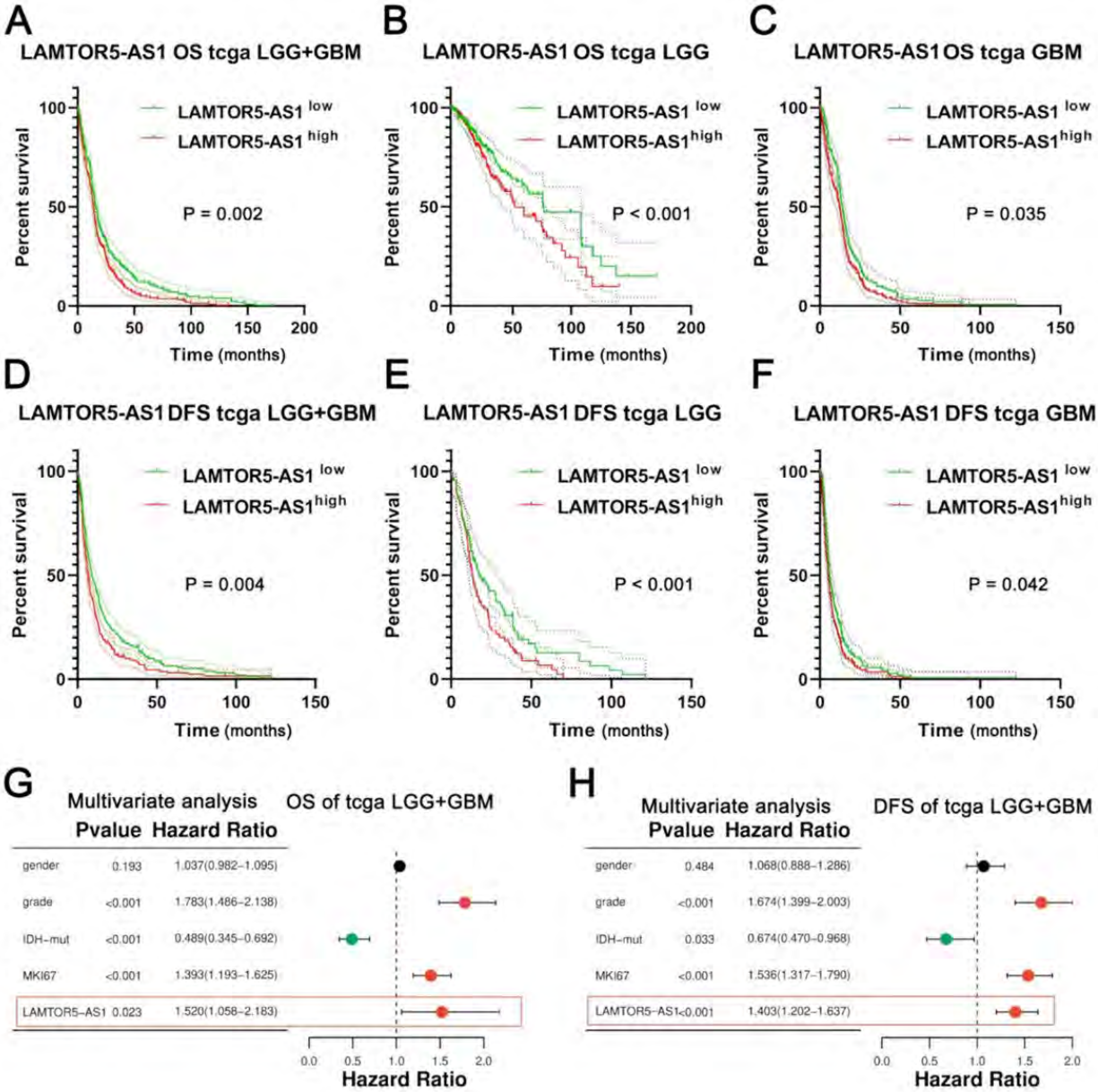

Fig. 3 Download full resolution image

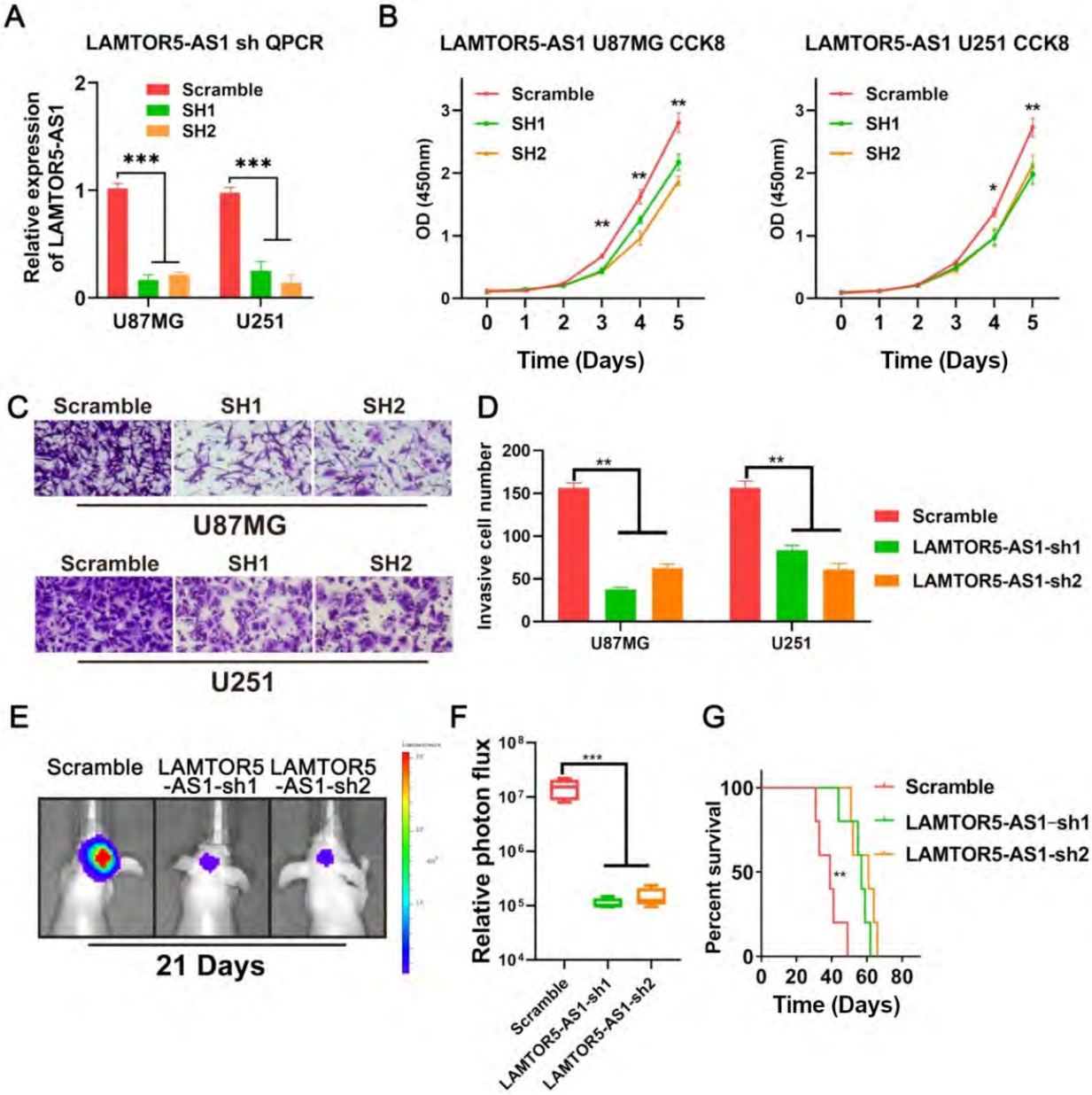

Fig. 4 Download full resolution image

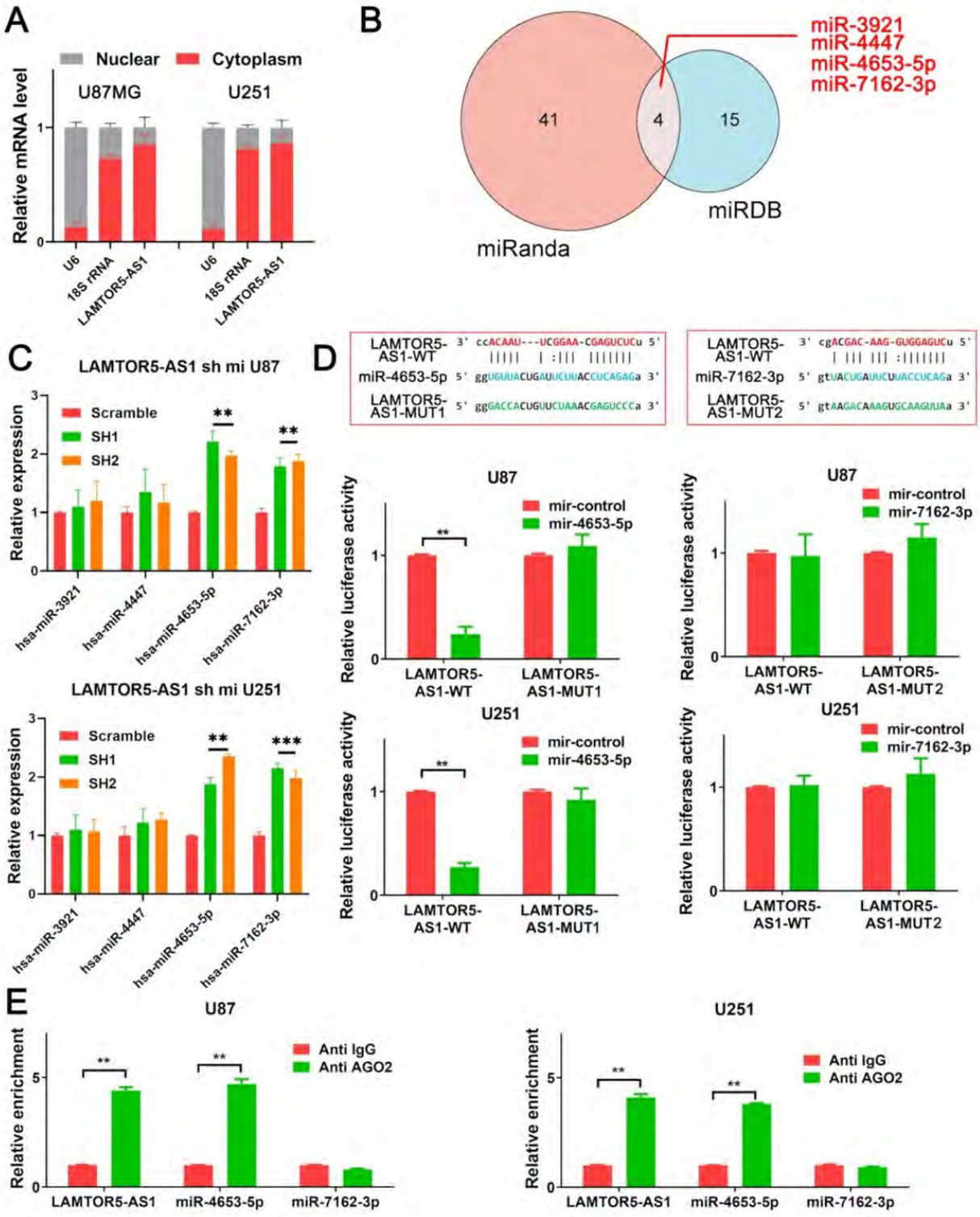

Fig. 5 Download full resolution image

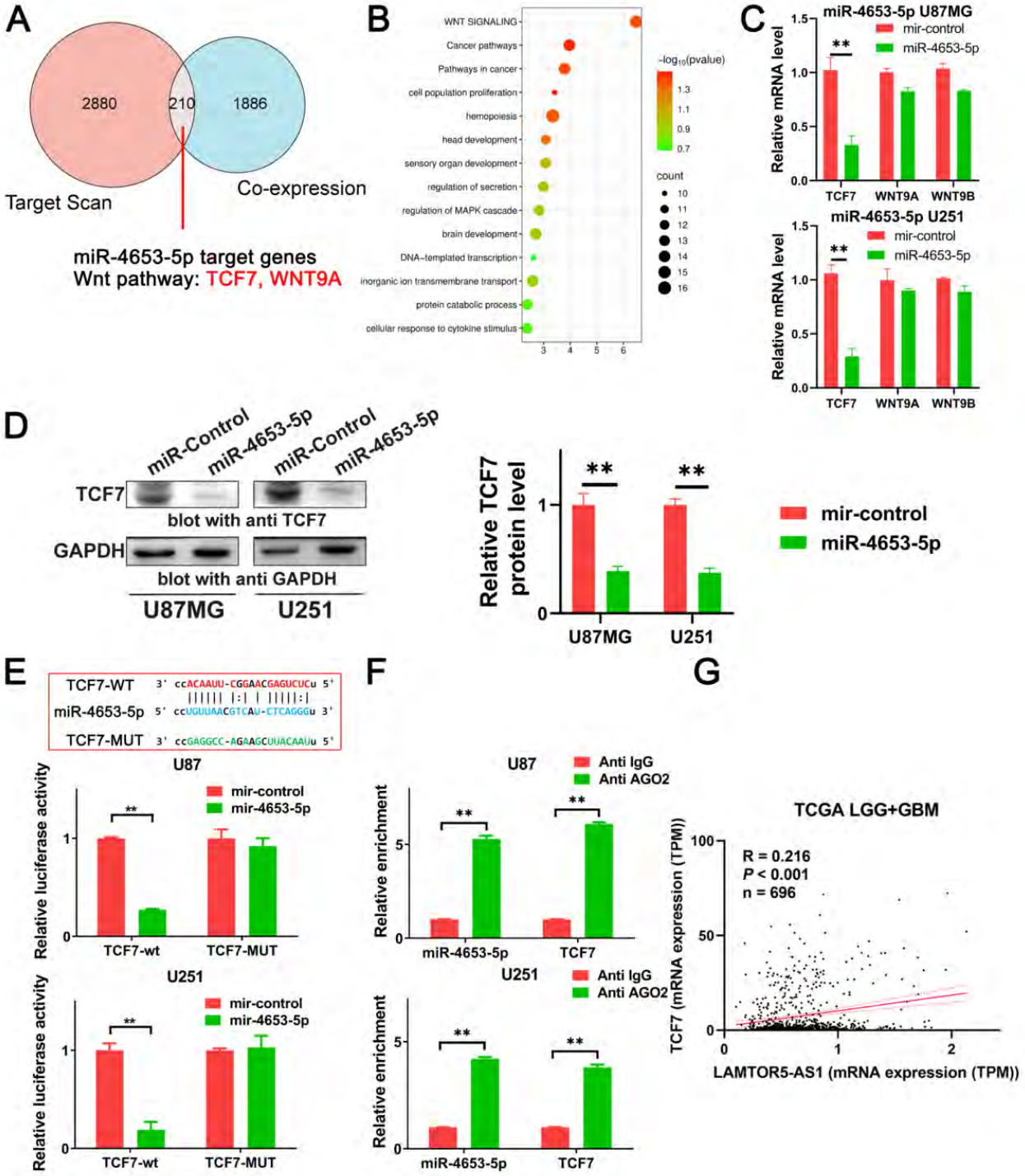
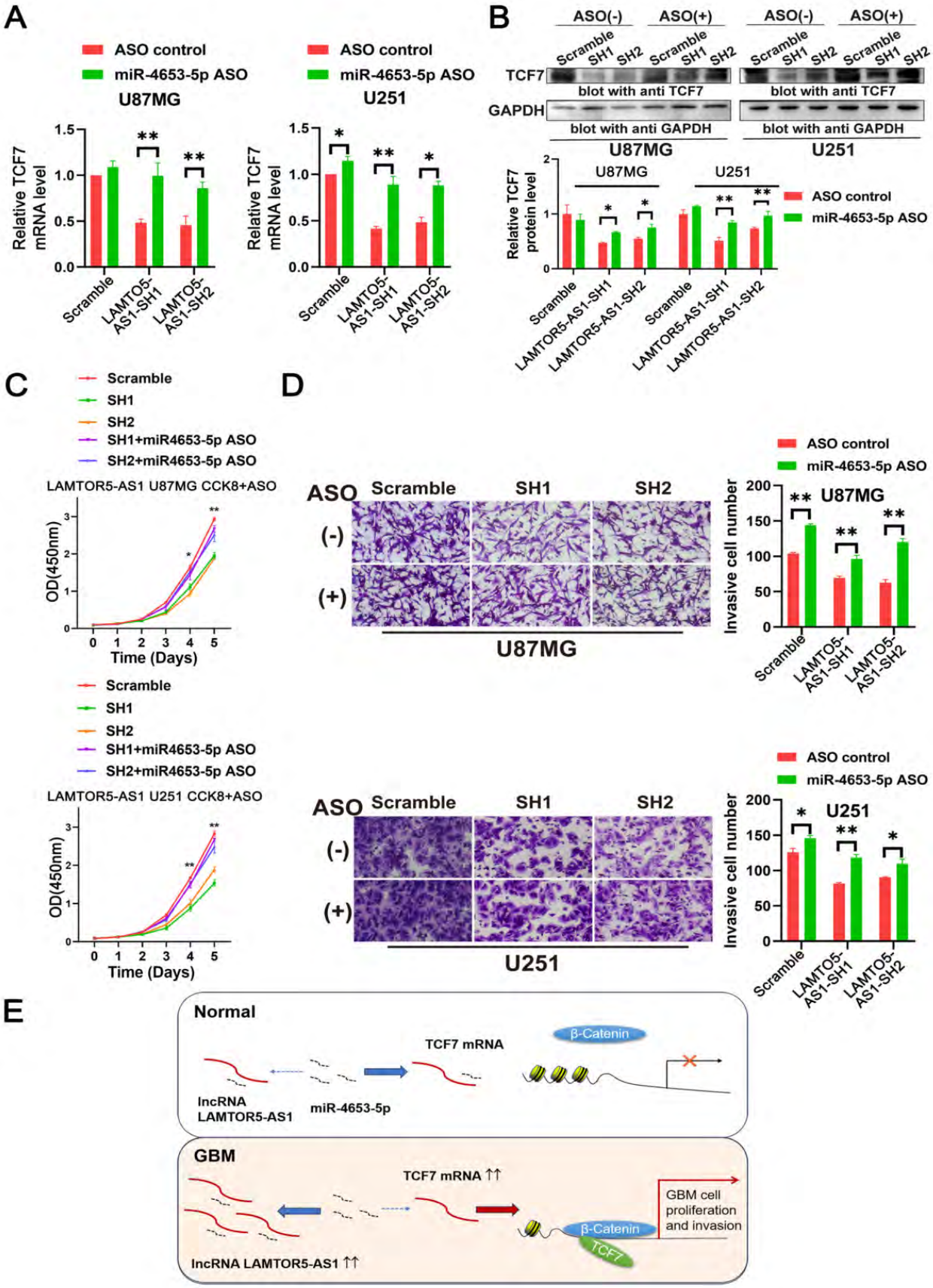
Fig. 6 Download full resolution image